CrystEngComm

Accepted Manuscript

ROYAL SOCIETY OF CHEMISTRY

www.rsc.org/crystengcomm

Effect of anion on Ag(I) meso-helical chains formed with 4,4'-dipyridyl ketone: solvent versus anion bridging and anion effects on the strength of ligand binding†

Komal M. Patil, Scott A. Cameron, Stephen C. Moratti and Lyall R. Hanton*

Received (in XXX, XXX) Xth XXXXXXXXX 20XX, Accepted Xth XXXXXXXXX 20XX
DOI: 10.1039/b000000x

The synthesis and characterisation by IR spectroscopy and elemental analysis of ten new Ag(I)–**L** complexes are described. Of these complexes nine are characterised by single crystal X-ray diffraction: $\{[Ag(\mathbf{L})](CF_3SO_3)\cdot^1/_2H_2O\}_\infty$ (**1**), $\{[Ag(\mathbf{L})](ClO_4)\cdot^1/_2H_2O\}_\infty$ (**2**), $\{[Ag_2(\mathbf{L})_2(CH_3CN)](ClO_4)_2\cdot 2CH_3CN\cdot H_2O\}_\infty$ (**3**), $\{[Ag_2(\mathbf{L})_2(CH_3CN)_2](ClO_4)_2\cdot CH_3CN\}_\infty$ (**4**), $\{[Ag_2(\mathbf{L})_2(CH_3CN)_2](PF_6)_2\cdot 2CH_3CN\}_\infty$ (**5**), $\{[Ag(\mathbf{L})_2](CF_3SO_3)\cdot^1/_2H_2O\}_\infty$ (**6**), $\{[Ag(\mathbf{L})_2](BF_4)\}_\infty$ (**7**) and $\{[Ag(\mathbf{L})_2](PF_6)\}_\infty$ (**8**) and $\{[Ag(\mathbf{L})_2](PF_6)\cdot 2CH_3CN\}_\infty$ (**9**). The primary structures of **1**–**6** were meso-helical one-dimensional (1D) polymers while **7** was a helical 1D polymer and **8** and **9** were (4,4) networks. Complexes **1**–**5** possessed 1:1 metal–to–ligand (M:L) ratios while complexes **6**–**9** possessed 1:2 M:L ratios. The meso-helical chains of the complexes **1** and **2** were di-μ-bridged at the Ag(I) nodes by the counteranions $CF_3SO_3^-$ and ClO_4^-, respectively, while the meso-helical chains of the complexes **3**–**5** were di-μ-bridged at the Ag(I) nodes by the CH_3CN molecules. The effect of counteranions and solvent molecules on delicate anion–Ag, π–π-stacking and argentophilic interactions has been studied through complexes **1**–**5**. The 1D chains of complexes **6** and **7** possessed monodentate **L** ligand sidearms. The uncoordinated N–donors of these sidearms were inclined towards the Ag(I) center of the adjacent chains and demonstrated narrower Ag–N_{py}–$Cg_{(pyridyl)}$ angles. In the case of complexes **8** and **9**, wider Ag–N_{py}–$Cg_{(pyridyl)}$ angles and stronger N···Ag interactions resulted in (4,4) nets. The effect of the size and the nature of the counteranions on the topology were studied through complexes **6**–**9**.

Introduction

1D architectures form an extensively explored area of coordination polymer chemistry. About 40% of the total reported coordination polymers in the last decade are 1D in nature. Yet there have been very few reviews dedicated to 1D coordination polymers between the years 1993 and 2010, for many researchers perhaps consider 1D coordination polymers to be structurally less attractive than their higher dimensional counterparts.[1] However, through weaker interactions these simple and seemingly less attractive structures possess the ability to demonstrate unusual and interesting architectures. In this regard, Ag(I) is particularly useful, and a significant number of 1D coordination polymers contain Ag(I), as its low dimensional and accommodating stereochemistry often allows it to interact with additional donor atoms from solvent or counteranion.[2]

Rigid, linear bridging ligands enable the formation of predictable arrays because of their configuration, coordination activity, and relative orientation of the donor groups. Rigid linear linking ligands such as 4,4'–bipyridine and pyrazine have already been extensively studied for designing linear 1D coordination polymers and higher dimensional networks.[3] Introduction of a bend in these ligands introduces a new variable to the study of the coordinating aspects of these linear linkers. The bend provides an opportunity to study lower dimensional structures such as helical,[4] meso-helical,[5, 6] zigzag[7-9] chains and other structures of current interest.[10] One simple bent ligand is 4,4'–dipyridyl ketone (**L**) (Figure 1). In the solid-state **L** contains a chiral axis passing through the carbonyl group of the ligand. NDDO calculations reported for **L** determined that the two rotational energy maxima for rotation of both pyridine rings through or orthogonal to the molecular plane are approximately 45 and 20 kJ mol^{-1}, respectively.[11] In solution, these two enantiomers readily interconvert from one form to another because of the low energy of conversion, effectively making them appear achiral.[12, 13] However in the solid-state, the conjugating effect between C=O and Py–rings and the hydrogen repulsion in the planar form provide resonance stability to this ligand.[11] The process of stabilisation "freezes" the racemates making **L** behave as a two-bladed chiral molecular propeller in the solid-state.[14] An analogous ligand, 4,4'–dipyridyl amine acts in a similar fashion as a two-bladed molecular propeller.[15] Surprisingly, there have been few examples of the use of **L** in

Department of Chemistry, Te Tari Hua-Ruanuku, University of Otago, P. O. Box 56, Dunedin 9054, New Zealand.

Fax: +643 479 7906; Tel: +643 479 7918; E-mail: lhanton@chemistry.otago.ac.nz

† Electronic supplementary information (ESI) available: Selected bond lengths and angles for complexes **1-9** CCDC reference numbers 982462–982470. For crystallographic data in CIF or other electronic format see DOI: 10.1039/b000000x

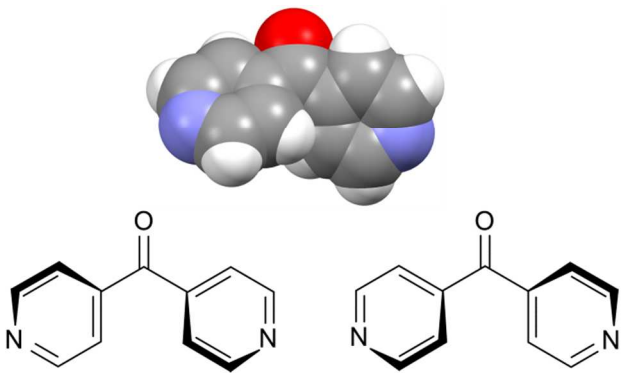

Figure 1 **Top:** View from the X-ray structure of **L** showing this ligand as a two-bladed molecular propeller;[16] **Bottom:** two enantiomers of **L**

coordination polymer chemistry. LaDuca and co-workers have reported the use of **L** as a linking ligand with $Cu(NO_3)_2$ forming three-fold double helices of $[Cu(\mathbf{L})]_n$[12] and with $AgNO_3$ forming zigzag 1D chains of $[Ag(\mathbf{L})(NO_3)]_n$.[13] The **L** ligand formed a pair of 1D meso-helical chains di (μ:κ^2O,O')-bridged at the Ag(I) nodes when a CF_3COO^- counteranion was employed. These chains extended their framework by virtue of weak π-π interactions.[17]

Linear and zigzag polymers are widely encountered in the literature. Helical polymers have gained added interest in the past decade because of their inherent chirality[18] while meso-helical polymers remain relatively uncommon. A meso-helix represents an alternative way, compared to a helix, of combining chiral components into an extended structure.[19] Thus, a lemniscate (∞) or figure of eight can be converted into a meso-helix by transforming it into the third-dimension (Figure 2).[20] This achiral 1D strand consists of alternate linkages of the *M*– and *P*–forms of the ligands to the metal center (M). The chain is thus represented as –*M*–(M)–*P*–(M)–*M*–(M)–*P*– and can sometimes be misinterpreted as a zigzag chain.[21, 22]

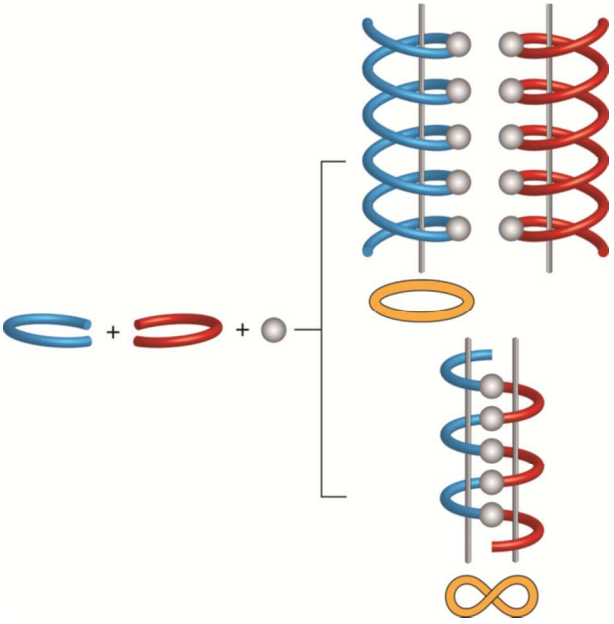

Figure 2 Schematic representation of formation of the helical and meso-helical chain. Enantiomeric ligands are represented as red and blue forms.

Herein we describe the use of the bent bridging ligand **L** to form two series of related coordination polymers of Ag(I) salts with varying M:L ratio (1:1 and 1:2). These coordination polymers were structurally characterised by single crystal X-ray diffraction, IR spectroscopy and elemental analysis. The first Ag(I) series comprised six 1:1 complexes (1–3, 3a, 4, 5) generated by employing the counteranions $CF_3SO_3^-$, ClO_4^-, BF_4^- and PF_6^-. Since all the 1:1 Ag–L complexes were meso-helical, 1D chains, the diversity in counteranions did not play a profound role in determining the primary structure. However, these coordination polymers provided an opportunity to study the delicate anion–Ag versus CH_3CN–Ag bridging interactions and their consequences for π–π-stacking and argentophilic interactions in this series of related 1D meso-helical chains. The second Ag(I) series comprised four related 1:2 complexes (6–9) generated by employing the counteranions $CF_3SO_3^-$, PF_6^- and BF_4^-. In contrast to the first series, the primary structure of these coordination polymers was influenced by the nature of the counteranion, which moderated the extent of interaction between the N-pyridyl (N_{py}) donor on the peripheral arms and the Ag(I) ion. The counteranion did not directly interact with the Ag(I) ion.

Results and discussion

Coordination polymers 1–9 were all prepared using the same 1:1 v/v CH_3CN:CH_3OH solvent system. Reactions were carried out in 1:1 and 1:2 M:L molar ratios. The products formed showed a considerable degree of sensitivity towards the nature of the counteranion and also the M:L ratio. For $AgCF_3SO_3$ and $AgBF_4$, two products were isolated and the final products had M:L ratios in agreement with the starting ratios as determined by microanalyses. For $AgPF_6$, regardless of the M:L ratio used a mixture of products was formed and a 1:1 and two 1:2 pseudo-polymorphic coordination polymers were isolated. For $AgClO_4$, regardless of the M:L ratio only polymorphic 1:1 products could be isolated. Even when a 2:1 M:L ratio was used only a 1:1 product was formed which was found to be a pseudo-polymorph of the other two 1:1 $AgClO_4$ products.

Synthesis and structure of $\{[Ag(L)](CF_3SO_3)\cdot{}^1/_2H_2O\}_\infty$, 1. A 1:1 molar reaction between $AgCF_3SO_3$ and **L** resulted in a tan solid. The microanalysis was consistent with the 1:1 formulation. Infrared studies of these samples confirmed the presence of **L** as the peaks at 1682 (ketonic C=O group), 3124–3053 (aromatic C–H stretching), 1611 and 1555 (C=C bending) and 759–660 cm^{-1} (aromatic C–H bending) were observed. The peak corresponding to C=O moiety of this complex was lower (1682 cm^{-1}) than observed in the free ligand (1731 cm^{-1}). The peaks corresponding to the stretching of the S=O, C–F, S–O and C–S bonds of the $CF_3SO_3^-$ counteranion were observed at 1330–1271, 1236–1018, 940–844 and 759–572 cm^{-1}, respectively. In infrared studies of $AgCF_3SO_3$, Johnston and Shriver have demonstrated that the peak at 1271 cm^{-1} arises from asymmetric SO_3 stretching, at 1236 cm^{-1} from symmetric

CF_3 stretching and at 760 cm^{-1} due to the CF_3 angle deformation and the symmetric C–S stretching.[23]

Complex **1** crystallised in the monoclinic space group *C*2/*c* with one Ag(I) cation, one complete **L** ligand, one $CF_3SO_3^-$ counteranion and half a H_2O of crystallisation in the asymmetric unit. Complex **1** formed a 1D meso-helical strand running along the [1 0 1] diagonal axis (Figure 3). The Ag(I) ion was essentially linear with an N–Ag–N angle of 175.72(6)°. The slight bend was a consequence of weak interactions between the Ag(I) cation and the O–atoms of adjacent $CF_3SO_3^-$ anions (Figure 3).[24] The pyridyl rings of **L** formed a two-bladed chiral propeller at an angle between the rings of 50.37(9)° and generated 1D strands. From the viewpoint of chirality, these 1D strands consisted of alternate linkages of the *M*– and *P*–forms of the ligands with the Ag(I) ions. The chain was thus represented as –*M*–(Ag)–*P*–(Ag)–*M*–(Ag)–*P*–, resulting in a meso-helical structure.[19]

Adjacent meso-helical chains were formed into anti-parallel pairs through a weak π–π interaction [centroid–to–centroid distance 3.803(2) Å; inter-planar dihedral angle 9.80(9)°, minimum interatomic distance 3.615(2) Å; minimum ring slippage between planes 1.664 Å]. The pairs of chains were di (μ:κ^2*O,O'*)-bridged by weak Ag···OSO_2CF_3 interactions which appeared to pull the Ag(I) ions closer together. The Ag···Ag distance was found to be 3.4704(16) Å. The bridging $CF_3SO_3^-$ anions on each side of the pairs of chains were linked together by hydrogen-bonding interactions with a H_2O of solvate [H···O distance of 1.94(4) Å corresponding to an O···O distance of 2.71(2) Å]. The pairs of chains interact with an adjacent pair of chains through π–π-interactions [centroid–to–centroid distance 3.766(2) Å, inter-planar dihedral angle 0°, minimum interatomic distance 3.746(2) Å; ring slippage between planes 1.680 Å] such that the rings involved in the interaction are in register every fifth pyridyl ring along the chains.

Synthesis and structure of $\{[Ag(L)](ClO_4)\cdot^1/_2H_2O\}_\infty$, 2. Evaporation of the solvents from a 2:1 molar reaction between $AgClO_4$ and **L** resulted in X-ray quality colourless crystals of **2**. However, microanalysis was consistent with a 1:1 formulation. Infrared studies of these samples confirmed the presence of **L** as the peaks at 1680 (ketonic C=O group), 3095 (aromatic C–H stretching), 1612–1555 (C=C bending) and 759–657 cm^{-1} (aromatic C–H bending) were observed. The presence of peaks at 1285, 1055, 952 and 691–619 cm^{-1} indicated the presence of ClO_4^-.

Complex **2** crystallised in the monoclinic space group *C*2/*c* with one Ag(I) cation, one complete **L** ligand, one ClO_4^- counteranion and half a H_2O of crystallisation in the asymmetric unit. It formed infinite 1D meso-helical strands running along the [1 0 1] diagonal axis (Figure 4). The Ag(I) ion was essentially linear with an N–Ag–N angle of 170.12(6)°.[24] The slight bend indicated a relatively weak interaction between an adjacent ClO_4^- anion at 2.727(2) Å and the Ag(I) cation. The Ag···$OClO_3$ interactions fell in the middle

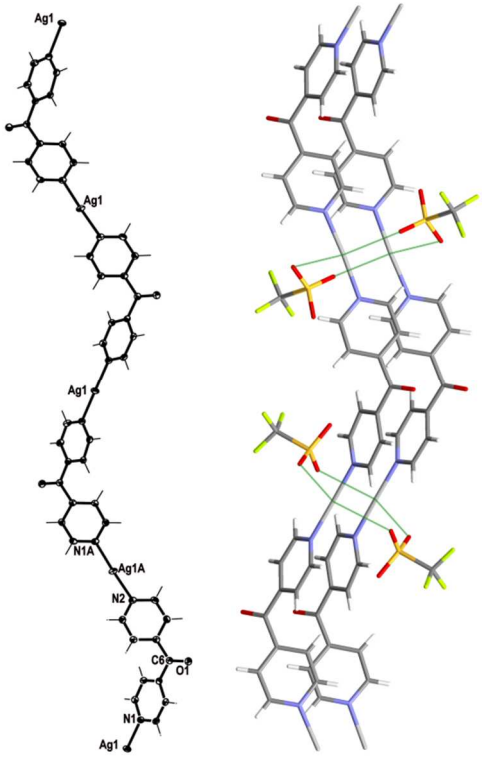

Figure 3 Left: View of the 1D cationic meso-helical polymeric strand of **1** running along the [1 0 1] direction (crystallographic numbering; ellipsoids 50% probability level). **Right:** View showing weak bridging in **1** by $CF_3SO_3^-$ counteranions. Only the major component of the disordered $CF_3SO_3^-$ counteranion is shown and H_2O molecules have been omitted for clarity.

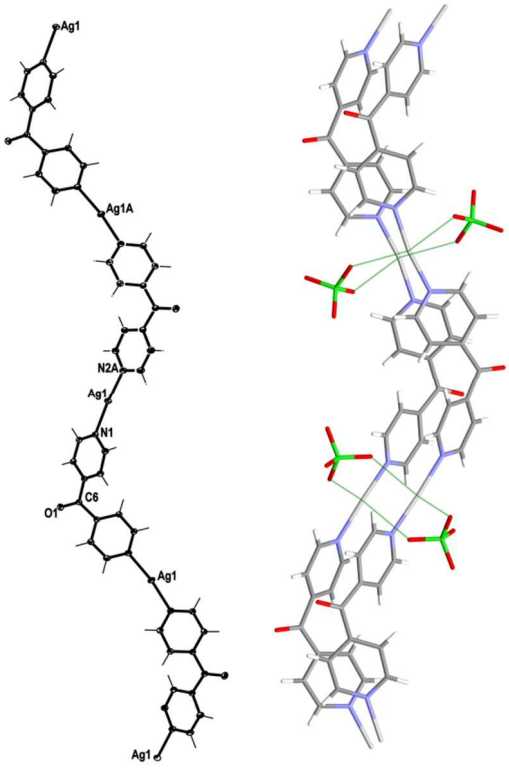

Figure 4 Left: View of the 1D cationic meso-helical polymeric strand of **2** running along the [1 0 1] direction (crystallographic numbering; ellipsoids 50% probability level). **Right:** View showing weak bridging in **2** by ClO_4^- counteranions. H_2O molecules were omitted for clarity.

of the range of Ag···O contact lengths [2.291–3.238 Å] for similar two-coordinated Ag···$OClO_3$ complexes as indicated by CSD database (Version 5.33).[25, 26] The pyridyl rings of **L** formed a two-bladed chiral propeller and registered an angle of 53.37(8)° between the planes of the rings. This complex possessed achiral meso-helical 1D chains similar to **1**.

The adjacent meso-helical chains were formed into anti-parallel pairs through two complementary interactions. One of which was weak π–π-interactions involving all the pyridine rings of the adjacent chain [centroid–to–centroid distance 3.763(2) Å, inter-planar dihedral angle 3.62(8)°, minimum interatomic distance 3.593(2) Å; minimum ring slippage between planes 1.589 Å]. The other involved the Ag ions of the chains being di(μ:κ^2*O,O'*)-bridged together by ClO_4^- anions on each side of the meso-helical pair (Figure 4). The Ag···Ag distance was 3.369(17) Å and the Ag···$OClO_3$ distances were 2.727(2) Å and 2.905(2) Å. The bridging ClO_4^- anions on each side of the pairs of chains were linked together by H-bonding interactions with a H_2O of solvate [H···O distance of 2.37(4) Å corresponding to an O···O distance of 3.039(3) Å]. There were no other noteworthy H-bonding interactions observed in the structure.

Synthesis and structure of {[Ag_2(L)$_2$(CH_3CN)](ClO$_4$)$_2$–·2CH_3CN·H_2O}$_\infty$, 3. Slow evaporation of the solvents from a 1:2 molar reaction between $AgClO_4$ and **L** resulted in X-ray quality colourless crystals of **3**. Again, the microanalysis was consistent with a 1:1 formulation. Infrared analysis revealed the peak corresponding to the C=O moiety of this complex was lower (1665 cm^{-1}) than observed in the **2** (1680 cm^{-1}). The peaks corresponding to the stretching and bending of aromatic rings of **L** and those for ClO_4^- were similar to **2**. Slow evaporation of the solvents from a 1:1 molar reaction between $AgBF_4$ and **L** resulted in colourless crystals of {[Ag_2(**L**)$_2$(CH_3CN)$_2$](BF_4)$_2$·CH_3CN·H_2O}$_\infty$ (**3a**) which were found to be isomorphous with **3** (experimental section).

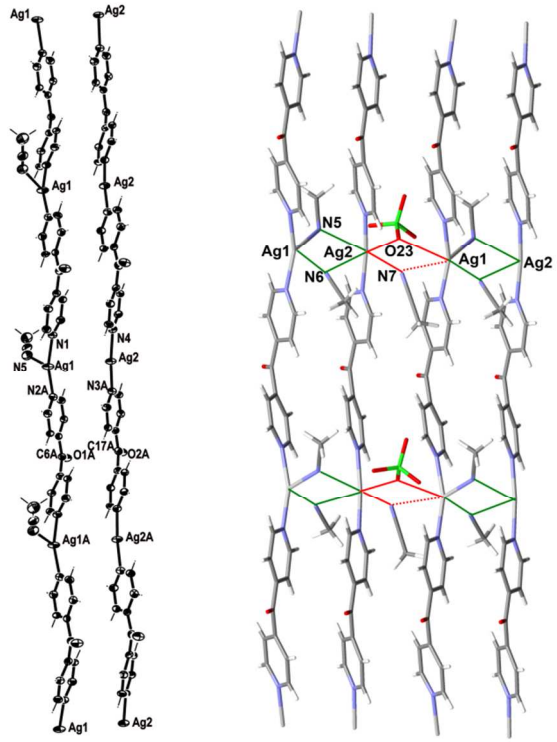

Figure 5 Left: View of the two distinct 1D cationic meso-helical polymeric strands of **3** running along the *c* axis (crystallographic numbering; ellipsoids 50% probability level). **Right:** A view showing bridging of two distinct meso-helical strands of **3** with CH_3CN molecules and weak bridging of the pair of strands with ClO_4^- and CH_3CN molecule. A non-interacting ClO_4^- counteranion and the H_2O molecules were omitted for clarity.

Complex **3** formed infinite 1D meso-helical strands along the *c* axis which through bridging interactions were formed into two-dimensional (2D) sheets in the *ac* plane. It crystallised in the monoclinic space group $P2_1/c$ with two crystallographically distinct Ag(I) cations, two complete **L** ligands, two ClO_4^- counteranions, three CH_3CN molecules and a H_2O of crystallisation in the asymmetric unit. The crystallographically distinct Ag(I) cations were present in different 1D meso-helical polymeric strands running parallel to each other along the *c* axis (Figure 5). One Ag(I) cation possessed a linear geometry by coordinating with two N–donors of the **L** ligand while the other Ag(I) cation possessed a T–shaped geometry by exhibiting additional coordination to a CH_3CN molecule. The linear Ag(I) cation displayed a slight bend and the N_{py}–Ag2–N_{py} angle measured 174.57(14) Å. This bend may have been the consequence of the weak Ag2···$OClO_3$ interactions [O23···Ag2 contact was 2.742(4) Å][24] and the weak N···Ag interactions with the free CH_3CN molecules [the N7···Ag2 contact was 2.853(5) Å and the N6···Ag2 contact was 3.023(4) Å]. The CH_3CN···Ag contacts for the two-coordinated Ag(I) cations were in the range of 2.555–3.265Å.[25, 26] A CH_3CN molecule coordinated to Ag1 at nearly perpendicular angles [the N(1)–Ag(1)–N(5) and N(5)–Ag(1)–N(2A) angles were 95.87(14)° and 94.84(14)°, respectively] and generated T–shaped Ag(I) nodes. The N_{CH3CN}–Ag distance was 2.505(4) Å. The N_{py}–Ag1–N_{py} angle of the T–shaped Ag(I) cation was 163.77(14)°. The T–shaped Ag1 displayed a distorted geometry and deviated from the plane (N5 N1 N2) by 0.2144 Å. The Ag–N_{py} bond lengths were found to be 2.171(4) Å and 2.177(4) Å while the Ag–N_{py} bond lengths of T–shaped Ag(I) were slightly elongated [the Ag1···N1 bond length was 2.203(4) Å and the Ag1···N2 bond length was 2.198(4) Å]. The bound CH_3CN displayed a bend in the C–N–Ag angle [147.0(4)°] by virtue of the weak interaction of CH_3CN with a Ag2 of a neighboring chain [the N···Ag2 contact was 3.121(4) Å]. The pyridyl rings of **L** formed a two-bladed chiral propeller and bridged the Ag(I) cores and formed infinite 1D meso-helical strands running along the *c* axis. The pyridyl rings of **L** coordinated to linear Ag(I) registered an angle of 40.3(2)° between the planes of the rings while the pyridine rings of the other **L** registered an angle of 46.0(2)° between the planes of the rings.

The linear and T–shaped Ag(I) ions were present in separate strands and formed a pair of dissimilar strands. This pair of strands was di(μ:κ^2*N*)-bridged by the CH_3CN molecules (Figure 5) and displayed weak π–π-stacking interactions [the centroid–to–centroid distances were 3.717(3) Å (inter-planar dihedral angle 5.5(2)°, minimum interatomic distance 3.601(3)

Å; minimum ring slippage between planes 1.293 Å) and 3.749(2) Å (inter-planar dihedral angle 1.8(2)°, minimum interatomic distance 3.701(2) Å; minimum ring slippage between planes 1.600 Å)]. These distances were registered every alternate pyridine ring throughout the pair of strands. One ClO_4^- counteranion bridged these pair of strands by virtue of C–H···anion interactions [the O11···H13 contact was 2.59 Å and the corresponding O11···H–C13 contact was 3.222(6) Å; the O14···H1 contact was 2.46 Å and the corresponding O14···H–C1 contact was 3.143(6) Å]. The Ag···Ag distance was 3.4858(6) Å. A pair of strands was linked with an adjacent pair of strands by the weak bifurcated bridging (μ:κ^2*O*) of ClO_4^- counteranion on one side [the O_3Cl–O23···Ag1 and the O_3Cl–O23···Ag2 contacts were 3.205(5) Å and 2.742(4) Å, respectively] and the weak bifurcated bridging (μ:κ^2*N*) of a CH_3CN molecule on the other side [the N7···Ag2 and N7···Ag1 contacts were 2.854(5) and 3.329(5) Å, respectively] (Figure 5). This asymmetric bridging was augmented by virtue of weak *π*–*π*-stacking interactions [centroid–to–centroid distance was 3.790(2) Å, inter-planar dihedral angle 1.8(2)°, minimum interatomic distance 3.746(2) Å; minimum ring slippage between planes 1.681 Å] and these interactions were registered every second pyridyl ring. The H_2O of crystallisation interacted with three ClO_4^- counteranions by virtue of H-bonding interactions. One interaction was relatively strong [H···O distance of 2.17(4) Å corresponding to an O···O distance of 2.966(6) Å] while the other two were weaker and interacted in a bifurcated fashion [H···O distances of 2.67(7) and 2.81(5) Å corresponding to O···O distances of 3.168(7) and 3.468(6) Å, respectively].

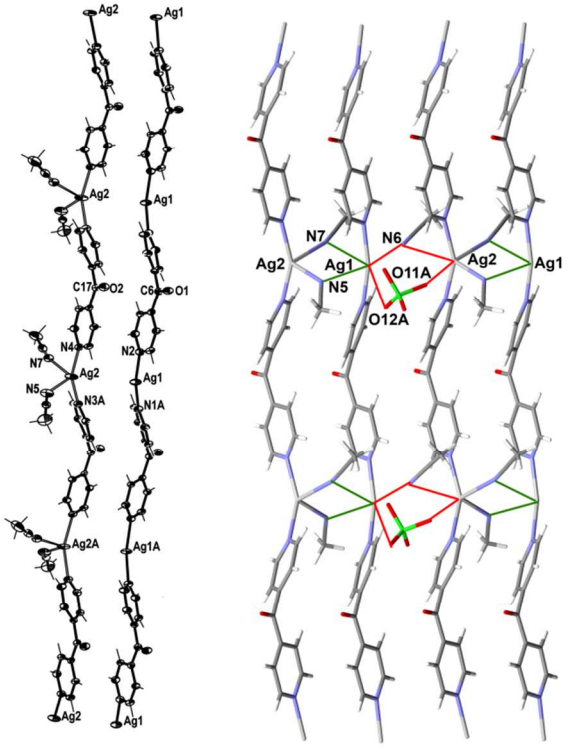

Figure 6 Left: View of the two distinct 1D cationic meso-helical polymeric strands of **4** running along the *c* axis (crystallographic numbering; ellipsoids 50% probability level). **Right:** A view showing bridging of two distinct meso-helical strands of **4** with CH_3CN molecules and weak bridging of the pair of strands with ClO_4^- and CH_3CN molecule. Only the major component of the disordered ClO_4^- counteranion is shown and the other ClO_4^- counteranion was omitted for clarity.

Synthesis and structure of {[Ag_2(L)$_2$(CH_3CN)$_2$](ClO_4)$_2$–·CH_3CN·H_2O}$_\infty$, 4. Slow evaporation of solvent from a solution of $AgClO_4$ and L in 1:1 M:L ratio resulted in X-ray quality colourless crystals of **4**. The infrared spectrum revealed that the peaks corresponding to the ketonic C=O group, stretching and bending of aromatic rings of **L** and ClO_4^- were similar with **2**.

Complex **4** formed infinite 1D meso-helical strands along the *c* axis which through bridging interactions were formed into 2D sheets in the *ac* plane. It crystallised in the monoclinic space group $P2_1/c$ with two crystallographically distinct Ag(I) cations, two complete **L** ligands, two ClO_4^- counteranions and three CH_3CN molecules in the asymmetric unit. The crystallographically distinct Ag(I) cations were present in different 1D meso-helical polymeric strands running parallel to each other along the *c* axis (Figure 6). One Ag(I) cation possessed a linear geometry by coordinating with two N–donors of the **L** ligand while the other Ag(I) cation possessed a four-coordinate geometry by exhibiting additional coordination to two CH_3CN molecules. The linear Ag(I) cation displayed a slight bend and the N_{py}–Ag1–N_{py} angle measured 165.85(18) Å. This bend may have been a consequence of the weak N···Ag interactions with the three CH_3CN molecules [the N···Ag contacts ranged between 2.887(7)–3.043(6) Å].[25, 26] The four-coordinated Ag(I) cation adopted a geometry between a seesaw and a trigonal pyramid as evidenced by the τ_4 value of 0.70.[27] The N5–Ag2 and N7–Ag2 distances were 2.414(6) Å and 2.657(6) Å, respectively. The N_{py}–Ag2–N_{py} angle of the four-coordinated Ag(I) cation was 155.14(17)°. The Ag1–N_{py} bond lengths were found to be equal [2.186(5) Å] while the Ag2–N_{py} bond lengths were slightly elongated [the Ag2···N3 bond length was 2.223(5) Å and the Ag2···N4 bond length was 2.222(5) Å]. The bound CH_3CN displayed a bend in the C–N–Ag angle [the C23–N5–Ag2 angle was 141.5(6)° and the C27–N7–Ag2 angle was 166.1(5)°] by virtue of the weak interaction of CH_3CN with the Ag1 of neighboring chain [the N5···Ag1 and N7···Ag1 contacts were 2.887(7) and 3.043(6) Å]. The pyridyl rings of **L** formed a two-bladed chiral propeller and bridged the Ag(I) cores and formed infinite 1D meso-helical strands running along the *c* axis. The pyridyl rings of **L** coordinated to the linear Ag(I) registered an angle of 45.6(3)° between the planes of the rings while the pyridine rings of the other **L** registered an angle of 50.7(3)° between the planes of the rings.

The linear and four-coordinated Ag(I) were present in separate strands and formed a pair of dissimilar strands. This pair of strands was di(μ:κ^2*N*)-bridged by CH_3CN molecules (Figure 6) and displayed weak *π*–*π*-stacking interactions [the centroid–to–centroid distances were 3.884(4) Å (inter-planar dihedral angle 5.8(3)°, minimum interatomic distance 3.770(4) Å; minimum ring slippage between planes 1.254 Å) and 3.945(4) Å (inter-planar dihedral angle 1.5(3)°, minimum interatomic distance 3.935(4) Å; minimum ring slippage between planes 1.939 Å)]. These distances were registered every alternate pyridyl ring throughout the pair of strands. The Ag···Ag distance was

3.694(3) Å. A pair of strands was linked to an adjacent pair of strands by the weak μ:κ^2*O,O'*-bridging of ClO_4^- counteranion on one side [the O_3Cl–O11A···Ag2 and the O_3Cl–O12A···Ag1 contacts were 3.201(16) Å and 2.953(13) Å, respectively] and the weak μ:κ^2*N*-bridging of a CH_3CN molecule on the other side [the N6···Ag1 and N6···Ag2 contacts were 2.886(6) and 3.217(6) Å, respectively] (Figure 6). This asymmetric bridging was augmented by virtue of weak *π*–*π*-stacking interactions [centroid–to–centroid distance was 3.884(4) Å (inter-planar dihedral angle 5.8(3)°, minimum interatomic distance 3.770(3) Å; minimum ring slippage between planes 1.254 Å) and 3.944(4) Å (inter-planar dihedral angle 1.5(3)°, minimum interatomic distance 3.935(4) Å; minimum ring slippage between planes 1.939 Å)] and these interactions were registered every alternate pyridyl ring. The Ag···Ag distance between the adjacent pair of strands was 4.139(3) Å.

Synthesis and structure of {[Ag$_2$(L)$_2$(CH$_3$CN)$_2$](PF$_6$)$_2$·2CH$_3$CN}$_\infty$, 5. A bulk reaction with a 1:2 M:L ratio of $AgPF_6$ and **L** resulted in the formation of a brown crystalline precipitate in moderate yield. However, the microanalysis of the bulk sample was consistent with a 1:1 formulation. Infrared studies of these samples confirmed the presence of **L** as the peaks at 1675 (ketonic C=O group), 1612 and 1555 (C=C bending) and 757–651 cm^{-1} (aromatic C–H bending) were observed. The very strong sharp peak at 821 cm^{-1} and strong sharp peak at 555 cm^{-1} indicated the presence of PF_6^- counteranions.[28]

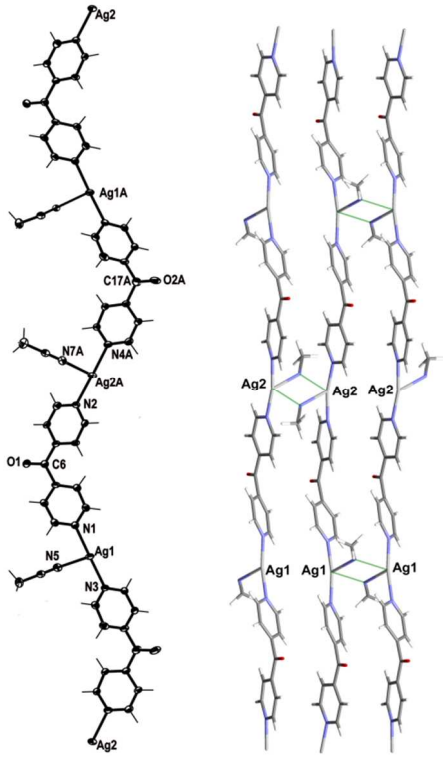

Figure 7 Left: View of the 1D cationic meso-helical polymeric strand of **5** running along the *b* axis (crystallographic numbering; ellipsoids 50% probability level). **Right:** A view showing bridging of two adjacent meso-helical strands of **5** with CH_3CN molecules. The PF_6^- counteranions, two uncoordinated CH_3CN molecule were omitted for clarity.

Complex **5** formed infinite 1D meso-helical strands along the *b* axis which through bridging interactions were formed into 2D sheets in the *ab* plane. It crystallised in the monoclinic space group $P2_1/c$ and the asymmetric unit consisted two crystallographically distinct Ag(I) cations, two complete **L** ligands, two PF_6^- counteranions and four CH_3CN molecules. The two crystallographically distinct Ag(I) cations and ligands were alternately present in the same 1D meso-helical strand despite it running along the crystallographic *b* axis (Figure 7). The Ag(I) cations displayed a pseudo T–shaped three-coordinated geometry by coordinating with two N_{py}–donors of two distinct **L** ligands and a CH_3CN molecule. The Ag1 deviated from the plane of the donor atoms (N3 N1 N5) by 0.120 Å while the Ag2 deviated from the plane (N2 N4 N7) by 0.160 Å. The Ag(I) nodes were bridged by two **L** ligands and 1D meso-helical strands were generated. The pyridyl rings of **L** formed a two-bladed chiral propeller. The pyridyl rings of the two **L** ligands registered the angles of 48.43(15)° and 48.05(15)° between the planes of the rings.

Two CH_3CN molecules coordinated to Ag1 and Ag2 at distances of 2.632(3) and 2.664(3) Å, respectively. The bound CH_3CN molecules displayed a bend in C–N–Ag angles [the C23–N5–Ag1 angle was 141.7(2) and the C27–N7–Ag2 angle was 143.6(2)°] by virtue of weak interactions with Ag(I) cations of neighboring chains. These interactions resulted in the di(μ:κ^2*N*)-bridging of the two antiparallel chains at alternate Ag(I) nodes by the bound CH_3CN molecules generating a 2D sheet in the *ab* plane (Figure 7). The N5···Ag1 contact was 2.772(3) Å while the N7···Ag2 contact was 2.751(3) Å. The bridging was augmented by very weak *π*–*π*-stacking interactions [the centroid–to–centroid contact was 3.9103(18) Å, (inter-planar dihedral angle 8.01(15)°, minimum interatomic distance 3.7430(18) Å; minimum ring slippage between planes 1.175 Å)]. The Ag···Ag distances at the bridged nodes [Ag1···Ag1 3.5632(4) Å and Ag2···Ag2 3.4709(4) Å] were considerably shorter than that at the non-bridged nodes [Ag1···Ag1 4.4372(5) Å and Ag2···Ag2 4.5448(5) Å]. The uncoordinated CH_3CN molecules interacted with the pyridine rings of the anti-parallel chains through weak N···H–C interactions ranged between 2.30–2.83 Å. There were no noteworthy H-bonding interactions observed in the structure.

Synthesis and structure of {[Ag(L)$_2$](CF$_3$SO$_3$)·$^1/_2$H$_2$O}$_\infty$, 6. A 1:2 molar reaction between $AgCF_3SO_3$ and **L** resulted in colourless crystals of **6**. The microanalysis was consistent with a 1:2 formulation. Infrared studies of these samples confirmed the presence of L as the peaks at 1675 (ketonic C=O group), 3200–3000 (aromatic C–H stretching), 1640–1554 (C=C bending) and 756–660 cm^{-1} (aromatic C–H bending) were observed. The peaks corresponding to the stretching of the S=O, C–F, S–O and C–S bonds of the $SO_3CF_3^-$ counteranion were observed at 1328–1284, 1222–1145, 949–830 and 660–634 cm^{-1}, respectively.

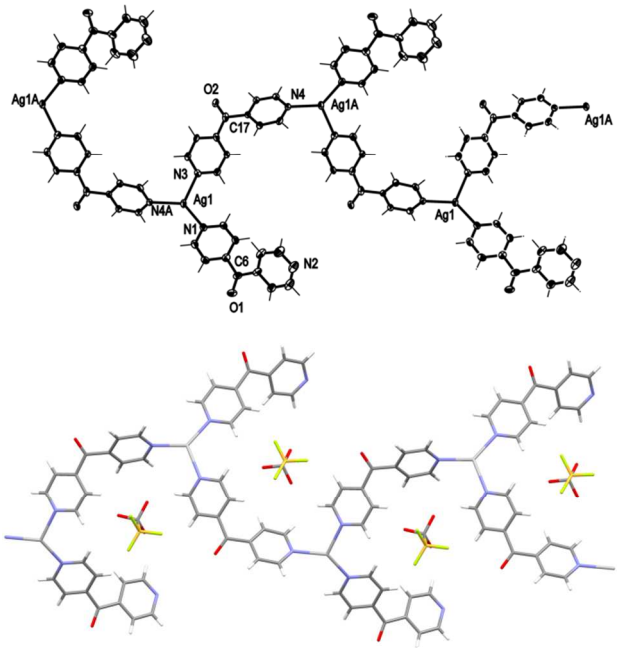

Figure 10 Top: View of the 1D cationic meso-helical polymeric strand of **6** running along the *c* axis (crystallographic numbering; ellipsoids 50% probability level). **Bottom:** View of a 1D meso-helical polymeric strand of **6** showing inclusion of $CF_3SO_3^-$ counteranions. Only the major component of the disordered $CF_3SO_3^-$ counteranion is shown and H_2O molecules have been omitted for clarity.

Complex **6** crystallised in the monoclinic space group *C*2/*c* to form a 1D meso-helical chain decorated with **L** arms (Figure 8). The chains ran along the *c* axis. The asymmetric unit contained one Ag(I) cation, two **L** ligands, one $CF_3SO_3^-$ counteranion and half a H_2O of crystallisation. The Ag(I) ions formed a distorted trigonal planar arrangement with three nitrogens of the pyridyl rings at angles of 112.8(2)°, 116.1(2)° and 127.5(2)° for N3–Ag1–N4, N1–Ag1–N3 and N1–Ag1–N4, respectively, while N2 remained uncoordinated forming the decorating arm of the meso-helix. The Ag(I) ion deviated by 0.251 Å from the plane of three bound N–donors. The weak interaction between $O_{H2O}\cdots$Ag1 [2.825(6) Å] distorted the planarity of AgN_3 moiety. In addition the H_2O molecule was H-bonded to the ketone O bridging two adjacent chains. The counteranions did not interact significantly with the polymeric stands.

The pyridyl rings of **L** formed a two-bladed chiral propeller. The **L** ligands which formed the polymeric backbone registered an angle of 48.8(4)° while the decorated **L** arms registered an angle of 58.6(4)° between the planes of the pyridine rings. The uncoordinated N2 of the dipyridyl ketonic arms showed a slight inclination towards Ag1 of an adjacent chain with N2$\cdots$Ag1 contact of 3.153(8) Å[29, 30] and registered an angle of 111.95° between the Ag(I)–$N2_{py}$–Cg_{py}. This long contact distance and very narrow angle indicated there is essentially no interaction between the pyridyl N2 and Ag1. The arrangement of the decorated arms created a cavity encompassing two $CF_3SO_3^-$ counteranions.

Synthesis and structure of $\{[Ag(L)_2](BF_4)\}_\infty$, 7. Slow evaporation of solvents from a solution of $AgBF_4$ and **L** in 1:2 M:L ratio resulted in X-ray quality colourless crystals of **7**. The microanalysis of the bulk reaction with similar molar and solvent ratio was consistent with a 1:2 formulation. Infrared studies of these samples confirmed the presence of **L** as the peaks at 1677 (ketonic C=O group), 3106–3054 (aromatic C–H stretching), 1608–1555 (C=C bending) and 756–660 cm^{-1} (aromatic C–H bending) were observed. The peaks at 1032, 756 and 520 cm^{-1} confirmed the presence of BF_4^- counteranion.

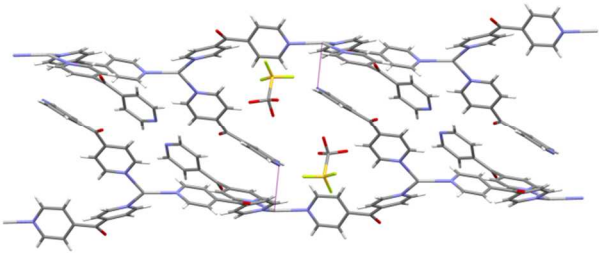

Figure 9 The anti-parallel meso-helical chains of complex **6** showing the disposition of the long N2$\cdots$Ag contact (shown in purple).

Complex **7** crystallised in monoclinic space group $P2_1/c$ to form infinite polymeric chains along the *b* axis. Each asymmetric unit contained one Ag(I) cation, two **L** ligands and one BF_4^- counteranion. One **L** ligand bridged the three coordinated Ag(I) nodes and extended the polymer to a 1D chain while the second **L** ligand interacted with Ag(I) through monodentate interactions and formed decorating side arms of the chain. Surprisingly, the 1D chain of **7** existed as a helix rather than a meso-helix. This was the only example of a helical chain for this entire series of compounds. Of necessity, both *M* and *P* forms of the helices were present in the centrosymmetric structure. The uncoordinated N2 of these side arms resided in the vicinity of Ag1 of the adjacent chain. The Ag1 bond distances to the other N_{py}–donors of 2.2121–

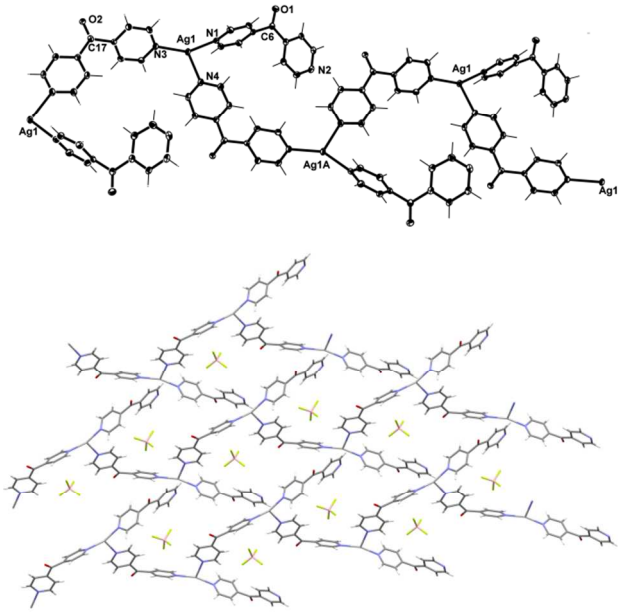

Figure 8 Top: View of the 1D cationic helical polymeric strand of **7** running along the *b* axis (crystallographic numbering; ellipsoids 50% probability level). **Bottom:** A view of (4,4) network of the **7** formed by virtue of N2$\cdots$Ag1 interactions between the adjacent meso-helical chains.

2.3861(17) Å were within the normal range. The Ag(I) cation adopted a slightly distorted trigonal-planar geometry with three N_{py} at the angle of 109.33(6)°, 149.54(6)° and 99.89(6)° for N3–Ag1–N4, N1–Ag1–N3 and N1–Ag1–N4, respectively. The Ag(I) ion deviated by 0.133 Å from the plane of three bound N–donors.

The pyridyl rings of **L** formed a two-bladed chiral propeller. The **L** ligands which formed the polymeric backbone registered an angle of 57.50(10)° while the decorated **L** arms registered an angle of 65.49(10)° between the planes of the rings. The two crystallographically distinct **L** ligands were pseudo enantiomers of each other. The uncoordinated N2 of the **L** side arm showed a significant inclination towards Ag1 with a N2···Ag1 contact of 2.6582(18) Å[29, 30] and registered an angle of 138.80° between the Ag(I)–N_{py}–Cg_{py}.[31] A search of the CSD identified 12 complexes with Ag(I)···N(pyridine) contacts

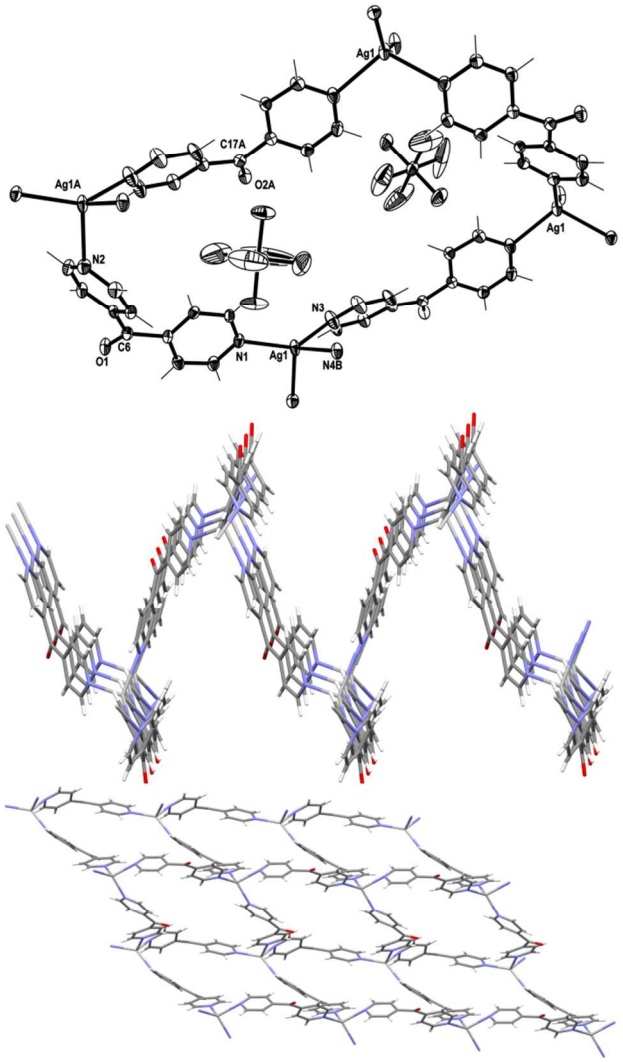

Figure 11 Top: View of a section of the (4,4) net of **8** displaying PF_6^- counteranions residing above and below the plane of the rhombus (crystallographic numbering; ellipsoids 50% probability level. **Middle:** A view in the *ab* plane showing a corrugated network of 8. PF_6^- counteranions were omitted for clarity. **Bottom:** A view in the *ac* plane showing a (4,4) network of complex **8**. PF_6^- counteranions were omitted for clarity.

in the range 2.60–2.70 Å. For 11 of these complexes the Ag(I)–N_{py}–Cg_{py} angle ranged from 132–141°, while one had a value of 125°. The consistency of the angles within this range suggested the presence of a weak interaction between the pyridyl N and Ag(I). By virtue of this close contact and the positioning of the decorated arms on the adjacent chains cavities existed in what appeared to be a pseudo (4,4) rhombic network (Figure 10). The four Ag1 ions occupied the corners of the rhombus and the adjacent sides of the network measured 11.102 Å and 11.471 Å. The four ligands of the rhombus were arranged such that two C=O groups of the opposite ligands, which were pseudo enantiomers of each other, pointed above the plane of the rhombus and in towards each other while the remaining two C=O groups of the ligands, which were also pseudo enantiomers, pointed below the plane and splayed away from each other (Figure 10). This arrangement caused the pseudo (4,4) network to be flat and achiral. The weak CH–π-interactions between C–H25···Cg2 (N2 containing pyridine) [The distance between H–centroid was 2.72 Å][32] and the weak π–π-interactions [the Cg2···Cg2 contact was 3.7572(16) Å, inter-planar dihedral angle 0°, minimum interatomic distance 3.736(16) Å; ring slippage between planes 1.525 Å][33] may have helped to facilitate the positioning of N2 near the Ag ion.

The BF_4^- counteranion resided within each cavity of the pseudo network by virtue of two weak attractive forces. A weak anion–π-interaction existed between BF_4^- and the pyridine ring containing N3 [F_3B-F···Cg 3.314(9) Å][34] and also weak CH–anion interactions existed between BF_4^- and pyridyl H atoms [the F···H contact distances ranged from 2.35-2.61 Å, and the corresponding F···C distances ranged from 3.027(2)-3.203(3) Å]. The cation–anion interactions stacked the adjacent layers of grids in an offset –A–B–A–B– fashion.

Synthesis and structure of $\{[Ag(L)_2](PF_6)\}_\infty$, 8 and $\{[Ag(L)_2](PF_6)\cdot 2CH_3CN\}_\infty$, 9. Slow evaporation of solvents from a solution of $AgPF_6$ and **L** in 1:2 M:L ratio resulted in X-ray quality colourless crystals of both **8** and **9**. The microanalysis of this sample was consistent with a 1:2 formulation. Infrared studies of these samples confirmed the presence of **L** as the peaks at 1686 and 1674 (ketonic C=O group), 1604 and 1556 (C=C bending) and 690–647 cm^{-1} (aromatic C–H bending) were observed. The environment around the ketonic C=O may have caused the C=O peak to split in two separate peaks. The very strong sharp peak at 818 cm^{-1} and strong sharp peak at 556 cm^{-1} indicated the presence of PF_6^- counteranions.[28]

Complex **8** crystallised in the monoclinic space group $P2_1/n$ to form an infinite 2D network in the *ac* plane. Each asymmetric unit of this complex contained one Ag(I) cation, two **L** ligands and one PF_6^- counteranion. The Ag(I) cation adopted a four-coordinated geometry between a seesaw and a trigonal pyramid as evidenced by the τ_4 value of 0.78.[27] The Ag1–N_{py} bonds were in the normal range from 2.244(3)–2.383(3) Å. The four N_{py} donors coordinated to the Ag(I) ion at angles between 94.52(11)–138.04(12)°. These pyridyl rings demonstrated more regular Ag(I)–N_{py}–Cg_{py} angles of between 150.51–175.69°. The **L** ligand formed a two-bladed chiral molecular propeller and the pyridyl rings of **L** registered angles of

54.44(16)° and 42.16(17)° between the planes of the rings. The two crystallographically distinct **L** ligands had the same pseudo enantiomeric form. Both the **L** ligands bridged the four coordinated Ag nodes and a corrugated (4,4) rhombic network was generated (Figure 11). The adjacent sides of the network measured 11.070(3) Å and 11.651(3) Å. The four ligands of the rhombus were arranged in an irregular way such that the C=O groups of three of the ligands pointed above and one pointed below the plane of the rhombus (Figure 11). The three ligands with the C=O groups which pointed above were of the same pseudo enantiomeric form while the one with the C=O group pointing below was of the other pseudo enantiomeric form. This arrangement caused the (4,4) network to be achiral and extremely corrugated and the planes of the adjacent facing rhomboids oriented themselves at angles of 66.3°. The adjacent sheets of the (4,4) network were interdigitated and stacked on top of each other in a –A–B–A– fashion along the *b* axis. These sheets interacted with each other by weak $O_{C=O}\cdots\pi$ interactions [O···Cg5 contact was 3.282(3) Å][35] and weak π–π-interactions [Cg4···Cg2 contact was 3.899(3) Å, inter-planar dihedral angle 12.50(17)°, minimum interatomic distance 3.739(3) Å; minimum ring slippage between planes 0.9035 Å].[33]

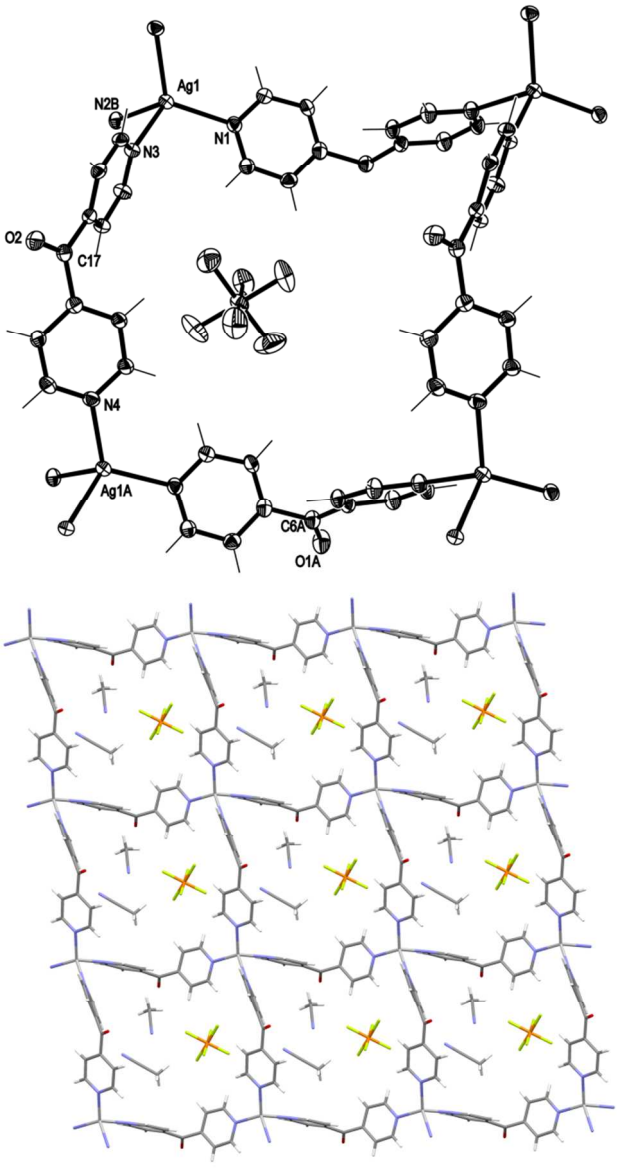

Figure 12 Top: View of a section of the (4,4) net of **9** displaying PF_6^- counteranion residing in the cavity (crystallographic numbering; ellipsoids 50% probability level). **Bottom:** A view in the *ab* plane showing a (4,4) network of **9**.

The two PF_6^- counteranions resided within the cavity being slightly above and below the plane of the rhombus by virtue of several weak anion–CH interactions [H···F contact distances between 2.44–2.97 Å] and strong anion–carbonyl interactions. The F11···C6 contact was 2.874(4) Å and the F14···C17 contact was 2.959(4) Å. A search of the CSD database suggested that for complexes containing pyridyl ketone like ligands, there were only two out of 204 observations which displayed a $F\cdots C_{C=O}$ contact below the van der Waals limit of 3.2 Å.[36, 37] In total in the CSD there are 422 observations of general O=C···F-PF_5^- interactions which range from 2.53 to 3.17 Å with a mean contact of 3.02 Å.[26, 27]

Complex **9** crystallised in the triclinic space group *P*–1 to form an infinite 2D network in the *ab* plane. Each asymmetric unit comprised one Ag(I) cation, two **L** ligands, one PF_6^- counteranion and two CH_3CN of crystallisation. The Ag(I) cation adopted a distorted tetrahedral geometry as evidenced by the τ_4 value of 0.91.[27] The four pyridine N–atoms coordinated to the Ag(I) ion at angles between 93.43(12)–119.90(12)° and interacted with the Ag(I) ions in the regular range of 2.268(4)–2.352(4) Å. These pyridyl rings demonstrated Ag(I)–N_{py}–Cg_{py} angles between 168.46–175.58°. The **L** ligand formed a two-bladed chiral molecular propeller and the pyridyl rings of L registered angles of 53.78(14)° and 77.2(9)° between the planes of the rings. The two crystallographically distinct **L** ligands were of the same pseudo enantiomeric form. Both the **L** ligand bridged the Ag nodes perpendicular to each other and a regular (4,4) rhombic network was generated (Figure 12). The adjacent sides of the network measured 10.950(7) Å and 11.108(7) Å. These distances corresponded to the length of crystallographic *a* and *b* axes. The four ligands of the rhombus, all of the same pseudo enantiomeric form, were arranged such that the C=O groups of the two ligands pointed above and two pointed below the plane of the rhombus (Figure 12). This arrangement gave a more regular network which was also chiral.[38, 39] The adjacent sheets of the (4,4) network, which were enantiomers of each other, were interdigitated and stacked on top of each other in a –A–B–A– fashion along the *c* axis.

The PF_6^- counteranions were embedded in the cavities of the (4,4) network by virtue of weak anion–π and CH–anion interactions. The distance between F15–to–centroid contact was 3.028(4) Å[34] while the distance between H1···F15 was 2.47 Å and the corresponding C9···F16 distance was 3.369(5) Å. No other noteworthy π–π-stacking and H-bonding interactions were observed.

Comparison of structures

In structures **1–9** the coordination environment of the Ag(I) ions ranged from linear to trigonal pyramidal. The **L** ligand bridged the Ag(I) cores and generated the primary structure of

1D meso-helical chains in complexes **1-6,** a helical 1D chain in complex **7** and 2D networks in complexes **8** and **9**. The 1D meso-helical polymers in **1** and **2** existed as pairs of chains di(μ:κ^2*O,O'*)-bridged with counteranions while in **3** –**5** they existed as 2D grids extended by bridging of the Ag(I) nodes of the 1D meso-helical polymers by counteranions and CH_3CN molecules. Complex **6** existed as a genuine 1D meso-helical polymer while complex **7** was a pseudo (4,4) network and the complexes **8** and **9** were (4,4) networks. The **L** ligand also acted as a two-bladed chiral molecular propeller within each solid-state structure such that the planes of the two pyridine rings intersected each other at an angle summarised in Table 1. The average twist in the planes of the pyridine rings was 52.6°. It is interesting to note that the pseudo-polymorphous complexes **3** and **4** and complexes **8** and **9** displayed large variations in these angles for only one of the ligands incorporated in the structures.

Table 1: Table showing angles between planes of pyridyl rings of ligand **L** in Ag–**L** complexes

Structure	*Angle (°)*
1	50.37(9)
2	53.37(8)
3	40.3(2) and 46.0(2)
4	45.6(3) and 50.7(3)
5	48.05(15) and 48.43(15)
6	48.8(4) and 58.6(4)
7	57.50(10) and 65.49(10)
8	54.44(16) and 42.16(17)
9	53.78(14) and 77.2(9)

The influence of the coordinating ability of the anions on the stoichiometry of the resultant Ag(I) complexes was demonstrated by our closely related series of coordination polymers.[40-42] The weakly coordinating $CF_3SO_3^-$ counteranion did not have an influence on the variation in stoichiometry as the stoichiometries of both the complexes **1** and **6** were consistent with the starting M:L ratios of 1:1 or 1:2, respectively. The ClO_4^- counteranions demonstrated stronger coordination to Ag(I) in presence of **L** as compared to the $CF_3SO_3^-$ counteranion. This prevented the formation of coordination polymers with different M:L ratios, as regardless of the starting M:L ratios, 2:1, 1:2 or 1:1, only the 1:1 complexes **2**, **3** and **4**, respectively, could be isolated. An excess of ClO_4^- present in the preparation of **2**, resulted in di(μ:κ^2*O,O'*)-bridging of the 1:1 polymer chain with ClO_4^-, while a deficiency as in case of **3** and **4**, instead resulted in di(μ:κ^2*N*)-bridging of the 1:1 chains with CH_3CN molecules. The starting M:L ratio of 1:2 in the reaction of $AgPF_6$ with **L** resulted in **5** with 1:1 and **8** and **9** with 1:2 M:L ratios. Owing to the non-coordinating nature of the PF_6^- counteranion, the 1:1 1D chains of **5** were di(μ:κ^2*N*)-bridged by CH_3CN molecules.

In the 1:1 M:L complexes, the AgN_2 moieties with the linear geometry displayed a slight bend in the N_{py}–Ag–N_{py} angles by virtue of weak Ag–anion interactions.[24] In the isostructural complexes **1** and **2**, the counteranions bridged the Ag(I) nodes of the adjacent meso-helical strands from both sides through di(μ:κ^2*O,O'*)-bridging of the Ag(I) cores of the adjacent strand. The bulky $CF_3SO_3^-$ counteranion of **1** displayed less influence on the bend in the linearity of Ag(I) cation [175.72(7)° vs. 170.12(6)°] and registered higher Ag···O distances when compared with the less bulky ClO_4^- anion (Table 2). The tighter bridging of the Ag(I) nodes by the ClO_4^- counteranions resulted in a shorter Ag···Ag contact distance and stronger *π*–*π*-interactions (Table 2). The ClO_4^- counteranions of the pseudo-polymorphous complexes **2**, **3** and **4** revealed various bridging modes. The adjacent strands of **2** were di(μ:κ^2*O,O'*)-bridged by ClO_4^- counteranions while the chains of **3** and **4** were weakly di(μ:κ^2*N*)-bridged by CH_3CN molecules. However in **3** and **4**, the ClO_4^- counteranions assisted the μ:κ^2*N* bridging of the CH_3CN molecules by bridging the adjacent pair of strands through μ:κ^2*O* and μ:κ^2*O,O'* interactions, respectively. The bridging of ClO_4^- counteranions along with the bifurcated bridging of CH_3CN molecule from the other side extended the structures of **3** and **4** to 2D grids. In **2** and **3**, the meso-helical chains bridged by ClO_4^- recorded shorter Ag···Ag contact distances but weaker *π*–*π*-interactions than the meso-helical strands bridged by CH_3CN. Surprisingly, the meso-helical strands of **4** demonstrated slightly tighter bridging by CH_3CN molecules but higher Ag···Ag contact and weaker *π*–*π*-interactions than the pseudo-polymorphous **3**. The CH_3CN molecules of **5** bridged the pair of meso-helical chains more tightly as compared to the bridging observed in **3**. This was evident by a shorter Ag···Ag contact in the case of **5** as compared to **3**. However, the *π*–*π*-interactions were found to be weaker in **5**. In **5**, the Ag···Ag contact at the bridged nodes was considerably shorter than that at the unbridged nodes, thus highlighting the effect of CH_3CN bridging.

Table 2: Table showing *π*–*π*, Ag···Ag and bridging interactions in the 1st series of Ag–**L** complexes

Complexes	***π*–*π***	**Ag···Ag**	**bridging**
1	3.803(2) Å	3.4704(16) Å	2.927(2) and 3.160(4) Å
2	3.763(2) Å	3.369(17) Å	2.727(2) and 2.905(2) Å
3	3.717(3) and 3.749(2) Å	3.4858(6) Å	2.742(4) and 3.023(4) Å; 2.505(4) and 3.121(4) Å
4	3.884(4) Å and 3.945(4) Å	3.694(3) Å	2.414(6) and 2.887(7) Å; 2.657(6) and 3.043(6) Å
5	3.9103(18) Å	3.5632(4) and 3.4709(4) Å	2.632(3) and 2.772(3) Å; 2.751(3) and 2.664(3) Å

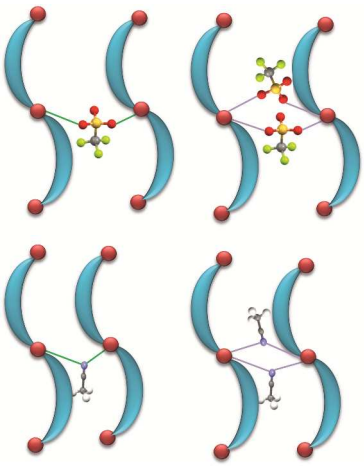

Figure 13 Top: Schematic representation of μ:κ^2*O,O'*-bridging (in green) and di(μ:κ^2*O,O'*)-bridging (in purple) of pairs of 1D strands by CF_3SO_3 counteranions at Ag(I) nodes **Bottom**: Schematic representation of μ:κ^2*N*-bridging (in green) and di(μ:κ^2*N*)-bridging (in purple) of pairs of 1D strands by CH_3CN molecules at Ag(I) nodes.

A search of the CSD database (Version 5.33) for Ag–anion interactions shorter than the sum of the van der Waals radii suggested that out of 1182 reported $AgClO_4$ complexes about 22% of the complexes demonstrate μ:κ^2*O,O'*-bridging of the counteranion while in about 7% of complexes the ClO_4^- counteranions displayed di(μ:κ^2*O,O'*)-bridging of the Ag(I) ions. Similarly, out of 1038 reported $AgCF_3SO_3$ complexes about 13% of complexes demonstrate μ:κ^2*O,O'*-bridging of the counteranion while in about 5% of complexes, the $CF_3SO_3^-$ counteranions displayed di(μ:κ^2*O,O'*)-bridging of the Ag(I) ions. Out of 959 reported $AgCH_3CN$ complexes, only 2.2% of complexes demonstrate μ:κ^2*N*-bridging of CH_3CN molecules while in 1.6% of complexes, the CH_3CN molecules displayed di(μ:κ^2*N*)-bridging of the Ag(I) ions.[25, 26]

In the 1:2 M:L complexes **6** and **7**, the uncoordinated N2 donor of the decorating **L** side arms of the strands displayed inclination towards the Ag(I) center on the adjacent polymeric chain and forced an unusual geometry on that metal center. The counteranions in both these complexes did not coordinate to the Ag(I) ion. However, the size of the counteranion played a critical role in elaborating the dimensionality of the chains. In the former complex, the bulkier $CF_3SO_3^-$ counteranion reduced the Ag(I)–N2$_{py}$–Cg$_{py}$ angle [111.95°] and thus restricted the coordination of N2 with the Ag(I) cation [the N2$\cdots$Ag contact was 3.152(7) Å]. By contrast, the less bulkier BF_4^- counteranion displayed less interference in the N$\cdots$Ag interactions [the N2$\cdots$Ag contact was 2.6595(18) Å and the Ag(I)–N2$_{py}$–Cg$_{py}$ angle was 138.80°] and thus facilitated the generation of a pseudo (4,4) network. The pyridyl rings of the decorating **L** side arms of **7** displayed more flexibility (as evident from Table **2**) and thus assisted the formation of the pseudo (4,4) network. The pyridyl rings of **8** displayed wider Ag(I)–N2$_{py}$–Cg$_{py}$ angles [150.51–175.69°] and shorter Ag–N contacts [2.244(3)–2.384(4) Å] and thus facilitated in the formation of a corrugated (4,4) network. The pyridyl rings of **9** displayed further wider Ag(I)–N2$_{py}$–Cg$_{py}$ angles [168.46–175.58°] and shorter Ag–N contacts [2.267(4)–2.353(4) Å] and thus helped form a regular (4,4) network. Out of 2523 examples in the CSD database (Version 5.33) for a search of Ag(I)–N$_{py}$–Cg$_{py}$ angles, 125 complexes were observed to be in the range of 89.8–140.8°. Scrutinizing the Ag(I)$\cdots$N$_{py}$ contact distances [ranged between 2.512–3.280 Å] in these complexes, it was observed that the distances are within the sum of the van der Waals radii for Ag–N [3.25 Å].[25, 26] There were 2427 observations with Ag(I)–N$_{py}$–Cg$_{py}$ angles between 144.6–180° and their Ag(I)$\cdots$N$_{py}$ distances range within 2.084-2.399 Å. This shows the wider the Ag(I)–N$_{py}$–Cg$_{py}$ angle, the stronger the Ag(I)$\cdots$N$_{py}$ interaction.

The C=O groups of the four ligands of the rhombus of **6** splayed outwards. In **7**, the C=O groups of the four ligands of the rhombus were arranged such that two C=O groups of the opposite ligands, which were pseudo enantiomers, pointed above the plane of the rhombus and in towards each other while the two C=O groups of the remaining ligands, which were also pseudo enantiomers, pointed below the plane and were splayed away from each other. This arrangement produced an achiral sheet. The rhombus of the 2D network of **9** has a regular orientation with two C=O groups pointing up and two pointing down and two CH_3CN molecules in each cavity. All four ligands of the rhombus were of the same pseudo enantiomeric form producing a chiral sheet. By contrast, the rhombus of the 2D network of **8** has irregular orientation with three C=O groups pointing up and one pointing down and no CH_3CN molecules in the structure. Three ligands of the rhombus had the same pseudo enantiomeric form while the remaining ligand was of the other pseudo enantiomeric form. This gave rise to an achiral sheet. Thus the irregular orientation of the C=O groups in **8** appeared to make the structure corrugated rather than flat while the vacillations of the C=O groups prevented the formation of true 2D networks in **6** and **7**. These differences may have been the cause of the embedding of the counteranions and the solvent molecules in the network cavities.

Conclusions

In conclusion, we have described two series of related coordination polymers of Ag(I) salts and L ligand with varying M:L ratio (1:1 and 1:2). The primary structure of the first Ag(I) series was not sensitive to counteranion. However, the delicate anion–Ag and CH_3CN–Ag bridging interactions showed subtle effect on *π*–*π*-stacking and argentophilic interactions. Owing to these delicate interactions, a transition from 1D meso-helical chains to 2D grids was observed. The second Ag(I) series displayed a remarkable sensitivity to counteranion showing a transition from ordered 1D meso-helical chains to 2D (4,4) nets.

Experimental section

Commercially available 4,4'–dipyridyl ketone was acquired from Chem Bridge. All chemicals were used as received without further purification. All solvents were of LR grade or above. The samples for microanalyses studies were dried under vacuum to remove volatile sample residues. Elemental microanalyses were carried out at the Campbell

Microanalytical Laboratory, University of Otago. All measured microanalyses results were within an uncertainty of 0.4%. Infrared (IR) spectra were recorded on a Perkin-Elmer Spectrum BX FT-IR system.

Caution! Although no problems were encountered in this work, transition metal perchlorates are potentially explosive. They should be prepared in small amounts and handled with care.

Reaction of L with $AgCF_3SO_3$ in 1:1 ratio

Solid $AgCF_3SO_3$ (13.94 mg, 0.054 mmol) dissolved in CH_3CN (0.8 mL) was added dropwise to a methanolic solution of **L** (10 mg, 0.054 mmol). The resultant solution was sonicated and allowed to evaporate slowly for a week to yield X-ray quality colourless crystals of $\{[Ag(\mathbf{L})](CF_3SO_3)\cdot{}^1/_2H_2O\}_\infty$ (Complex **1**) which on drying *in vacuo* converted into a tan powder. Yield: 11 mg, 46%; Analysis found: C 32.95, H 1.89 and N 6.29; Calculated for the formula $C_{12}H_8O_4N_2SF_3Ag$: C 32.67, H 1.83 and N 6.35; Selected IR/cm^{-1}: 3124–3053 (w, br), 1682 (m, sh), 1611 (w, sh), 1555 (w, sh), 1423 (m, sh), 1330–1271 (s, br), 1236 (s, br), 1216 (s, br), 1150 (s, br), 1105 (s, br), 1018 (s, sh), 940 (m, sh), 878–844 (w, br), 759 (m, sh), 660 (m, sh), 630 (s, sh), 572 (m, sh), 515 (s, sh).

Reaction of L with $AgClO_4\cdot H_2O$ in 1:2 ratio

Solid $AgClO_4\cdot H_2O$ (22.5 mg, 0.108 mmol) dissolved in CH_3CN (1.5 mL) was added dropwise to methanolic solution of **L** (10 mg, 0.054 mmol). The resultant solution was sonicated and allowed to stand for a week to yield X-ray quality colourless crystals of $\{[Ag(\mathbf{L})](ClO_4)\cdot{}^1/_2H_2O\}_\infty$ (Complex **2**) which on drying *in vacuo* converted into a tan powder. Yield (based on **L**): 10 mg, 47%; Analysis found: C 33.51, H 2.25 and N 7.61; Calculated for the formula $C_{11}H_8O_5N_2ClAg$: C 33.75, H 2.06 and N 7.16; Selected IR/cm^{-1}: 3095 (w, br), 1680 (m, sh), 1612 (w, sh), 1555 (w, sh), 1285 (m, br), 1055 (s, br), 952 (m, sh), 759 (m, sh), 691 (m, sh), 657 (s, sh) and 619 (s, sh).

Reaction of L with $AgClO_4\cdot H_2O$ in 2:1 ratio

Solid $AgClO_4\cdot H_2O$ (11.2 mg, 0.054 mmol) dissolved in CH_3CN (1 mL) was added dropwise to methanolic solution of **L** (20 mg, 0.108 mmol). The resultant solution was sonicated and allowed to evaporate slowly for a week to yield X-ray quality colourless crystals of $\{[Ag_2(\mathbf{L})_2CH_3CN](ClO_4)_2\cdot 2CH_3CN\text{–}\cdot H_2O\}_\infty$ (Complex **3**) which on drying *in vacuo* converted into a tan powder. Yield (based on Ag(I)): 11 mg, 50%; Analysis found: C 34.26, H 2.51 and N 7.06; Calculated for the formula $C_{11}H_8O_5N_2ClAg\cdot{}^1/_2CH_3OH$: C 33.89, H 2.47 and N 6.87; Selected IR/cm^{-1}: 3101 (w, br), 1665 (m, sh), 1609 (w, sh), 1556 (w, sh), 1286 (m, br), 1056 (s, br), 950 (m, sh), 758 (m, sh), 688 (m, sh), 659 (s, sh) and 620 (s, sh).

Reaction of L with $AgBF_4$ in 1:1 ratio

Solid $AgBF_4$ (21.2 mg, 0.108 mmol) dissolved in CH_3CN (1.5 mL) was added dropwise to methanolic solution of **L** (20 mg, 0.108 mmol). The resultant solution was sonicated and allowed to stand for a week to yield colourless crystals of $\{[Ag_2(\mathbf{L})_2(CH_3CN)_2](BF_4)_2\cdot CH_3CN\cdot H_2O\}_\infty$ (Complex **3a**) which on drying *in vacuo* converted into a tan powder. The crystals were twinned and of poor quality. However, these crystals were found to be isomorphous to Complex **3**. [a = 7.5055(8) Å, b = 19.063(3) Å and c = 23.000(3) Å; α = 90°, β = 91.312(4)° and γ = 90°; V = 3290(1) $Å^3$] Yield: 21 mg, 51%; Analysis found: C 35.04, H 2.03 and N 7.42; Calculated for the formula $C_{11}H_8ON_2BF_4Ag$: C 34.87, H 2.13 and N 7.39; Selected IR/cm^{-1}: 3108 (w, br), 1682 (m, sh), 1609 (w, sh), 1554 (w, sh), 1417 (m, sh), 1282 (m, br), 1162 (w, sh), 1034 (s, br), 879 (m, sh), 760 (m, sh), 658 (s, sh) and 520 (s, sh).

Reaction of L with $AgClO_4\cdot H_2O$ in 1:1 ratio

Solid $AgClO_4\cdot H_2O$ (11.3 mg, 0.054 mmol) dissolved in CH_3CN (1.5 mL) was added dropwise to methanolic solution of **L** (10 mg, 0.054 mmol). The resultant solution was sonicated and allowed to stand for a week to yield X-ray quality colourless crystals of $\{[Ag_2(\mathbf{L})_2(CH_3CN)_2](ClO_4)_2\cdot CH_3CN\}_\infty$ (Complex **4**) which on drying *in vacuo* converted into a tan powder. Yield: 15 mg, 71%; Analysis found: C 33.51, H 2.25 and N 7.61; Calculated for the formula $C_{11}H_8O_5N_2ClAg$: C 33.75, H 2.06 and N 7.16; Selected IR/cm^{-1}: 3102 (w, br), 1675 (m, sh), 1609 (w, sh), 1554 (w, sh), 1281 (m, br), 1061 (s, br), 951 (m, sh), 758 (m, sh), 688 (m, sh), 656 (s, sh) and 620 (s, sh).

Reactions of L with $AgPF_6$ in 2:1 ratio

Reaction **1**: Solid $AgPF_6$ (13.2 mg, 0.054 mmol) dissolved in CH_3CN (4 mL) was added dropwise to a 4 mL methanolic solution of **L** (20 mg, 0.108 mmol). The resultant clear solution was stirred overnight and concentrated in volume to 2 mL. Addition of 0.5 mL of diethyl ether yielded a brown crystalline precipitate which was filtered, washed with diethyl ether and dried *in vacuo*. Yield (based on Ag(I)): 13 mg, 55%. X-Ray quality colourless crystals of $\{[Ag_2(\mathbf{L})_2(CH_3CN)_2]\text{–}(PF_6)_2\cdot 2CH_3CN\}_\infty$ (Complex **5**) were grown by slow evaporation of solvents (1:1 v/v CH_3CN:CH_3OH) from the solution of $AgPF_6$ (6.9 mg, 0.027 mmol) and **L** (10 mg, 0.054 mmol). Analysis found: C 33.43, H 2.34 and N 7.81; Calculated for the formula $C_{11}H_8ON_2PF_6Ag\cdot CH_3OH\cdot CH_3CN$: C 32.96, H 2.96 and N 8.24; Selected IR/cm^{-1}: 3629 (w, br), 1675 (m, sh), 1612 (w, sh), 1555 (w, sh), 1418 (m, sh), 1284 (m, sh), 1160 (w, sh), 1134 (w, sh), 881 (m, sh), 821 (vs, sh), 757 (m, sh), 690 (m, sh), 651 (s, sh) and 555 (s, sh).

Reaction **2**: Solid $AgPF_6$ (13.2 mg, 0.054 mmol) dissolved in CH_3CN (1 mL) was added dropwise to methanolic solution of **L** (20 mg, 0.108 mmol). The resultant solution was sonicated and allowed to evaporate slowly for a week to yield X-ray quality colourless crystals of $\{[Ag(\mathbf{L})_2](PF_6)\}_\infty$ (Complex **8**) and $\{[Ag(\mathbf{L})_2](PF_6)(CH_3CN)_2\}_\infty$ (Complex **9**) which on drying *in vacuo* converted into a tan powder. Yield (based on Ag(I)): 20 mg, 60%. Analysis found: C 42.65, H 2.69 and N 9.11; Calculated for the formula $C_{22}H_{16}O_2N_4PF_6Ag$: C 42.54, H 2.60 and N 9.02; Selected IR/cm^{-1}: 1686 (m, sh), 1674 (m, sh), 1604 (w, sh), 1556 (w, sh), 1494 (w, sh), 1413 (m, sh), 1281 (m, sh), 1158 (w, sh), 949 (w, sh), 818 (vs, sh), 690 (m, sh), 647 (s, sh) and 556 (s, sh).

Reaction of L with $AgCF_3SO_3$ in 2:1 ratio

Solid $AgCF_3SO_3$ (13.94 mg, 0.054 mmol) dissolved in CH_3CN (1 mL) was added dropwise to methanolic solution of **L** (20

mg, 0.108 mmol). The resultant solution was sonicated and allowed to evaporate slowly for a week to yield X-ray quality colourless crystals of $\{[Ag(\mathbf{L})_2](CF_3SO_3)\cdot{}^1/_2H_2O\}_\infty$ (Complex **6**) which on drying *in vacuo* converted into a tan powder. Yield (based on Ag(I)): 22 mg, 65%; Analysis found: C 44.47, H 2.84, N 9.00, and S 4.91; Calculated for the formula $C_{23}H_{16}O_5N_4SF_3Ag$: C 44.18, H 2.58, N 8.96, and S 5.13; Selected IR/cm^{-1}: 3200–3000 (w, br), 1675 (m, sh), 1640 (w, sh), 1604 (w, sh), 1554 (w, sh), 1410 (m, sh), 1328 (m, sh), 1284 (m, sh), 1263 (s, sh), 1222 (m, sh), 1145 (m, sh), 1058 (s, sh), 1029 (s, sh), 949 (m, sh), 879 (m, sh), 830 (m, sh), 756 (m, sh), 660–634 (s, br).

Reaction of L with $AgBF_4$ in 2:1 ratio

Under a blanket of Ar gas, the methanolic solution (4 mL) of **L** (40 mg, 0.216 mmol) was added to 4 mL of CH_3CN solution of $AgBF_4$ (21.2 mg, 0.108 mmol). The resultant solution was allowed to react overnight. Addition of 0.5 mL of diethyl ether to this solution resulted in colourless crystalline solid which was filtered and dried *in vacuo*. Yield (based on Ag(I)): 28 mg, 43%); Analysis found: C 48.17, H 3.07 and N 10.18; Calculated for the formula $C_{22}H_{16}O_2N_4F_4BAg\cdot CH_3CN$: C 47.72, H 3.17 and N 11.59; Selected IR/cm^{-1}: 3106–3054 (w, br), 1677 (m, sh), 1608 (w, sh), 1555 (w, sh), 1409 (m, sh), 1282 (m, sh), 1160 (w, sh), 1032 (s, br), 756 (m, sh), 660 (s, sh), 520 (m, sh).

Solid $AgBF_4$ (10.6 mg, 0.054 mmol) dissolved in CH_3CN (1 mL) was added dropwise to methanolic solution of **L** (20 mg, 0.108 mmol). The resultant solution was sonicated and allowed to evaporate slowly for a week to yield X-ray quality colourless crystals of $\{[Ag(\mathbf{L})_2](BF_4)\}_\infty$ (Complex **7**).

X-Ray Data Collection and Structure Solution

Crystallographic data are summarised in Table 3. Selected bond lengths and angles of complexes **1-9** are available in supplementary material along with a description of how the disordered components of the complexes were treated. X-Ray diffraction data were collected at the University of Otago on a Bruker APEX II CCD diffractometer with graphite monochromated Mo-Kα (λ = 0.71073 Å) radiation. Intensities were corrected for Lorentz and polarisation effects and multiscan absorption corrections were applied to all structures. The structures were solved by direct methods SHELXS[43, 44] or SIR-97[45] and refined on F^2 using all data by full-matrix least-squares procedures SHELXL 97[43]. Non-hydrogen atoms were refined with anisotropic thermal parameters. Hydrogen atoms were placed in ideal positions except for the hydrogen atoms of the H_2O molecules in **1**, **2**, **3**, **4** and **6** which were located from the Fourier synthesis maps. In **1**, the $CF_3SO_3^-$ anion was disordered over two sites with site occupancy of 0.36 and 0.64. This $CF_3SO_3^-$ anion and H_2O molecule were modelled using DFIX constraints. In **4**, both ClO_4^- anions were disordered (50%). A very disordered CH_3CN of solvent was removed from the structure using the SQUEEZE procedure of PLATON[46] as it could not be modelled. Analysis of the X-ray data indicated that crystals might carry a well-defined twin. However, a twin law that superimposed all or half of the reflections could not be found. The twinning was evident in both data collections for **4**. As a result the precision of the data for 4 was not high. The crystals of **5** were of poor quality. Two different data sets for **5** were collected and solved, both of which were of poor quality because of weakly diffracting crystals. The solution reported herein represents the best quality solution. A CH_3CN molecule in **5** was disordered and the C and N atoms of this molecule were refined isotropically and the hydrogen atoms of this molecule were not placed. The disordered CH_3CN molecule was modelled with site occupancy of 0.6 and 0.4 and additional restraints were used to maintain the linearity. A $CF_3SO_3^-$ anion was disordered with site occupancy of 0.51 and 0.49. The F and O atoms of this molecule were refined isotropically. In **8**, the PF_6^- anion was disordered on four fold axis over two sites with site occupancy of 0.35 and 0.65. This PF_6^- anion was modelled using DFIX constraints. All calculations were performed using the WinGX[47] interface. Detailed analyses of the extended structure were carried out using PLATON[46] and MERCURY (Version 3.0)[26, 48] Crystallographic data are listed in the appendix.

Acknowledgements

We acknowledge the Department of Chemistry for the award of Master's Scholarship and thank the University of Otago for publication bursary (to KMP). We thank Professor Geoff Jameson for assistance with the twinning in **4**. Lisa Bucke is thanked for her assistance in preparing Figure **2**.

Notes and References

1. W. L. Leong and J. J. Vittal, *Chem. Rev.*, 2011, 111, 688-764.
2. C. K. Chen, B. Su, C. , *Aust. J. Chem.*, 2006, 59, 3-18
3. D. Visinescu, M. Andruh, A. Müller, M. Schmidtmann and Y. Journaux, *Inorg. Chem. Commun.*, 2002, 5, 42-45.
4. M.-L. Tong, X.-M. Chen, B.-H. Ye and S. W. Ng, *Inorg. Chem.*, 1998, 37, 5278-5281.
5. L. Hou, W.-J. Shi, Y.-Y. Wang, B. Liu, W.-H. Huang and Q.-Z. Shi, *CrystEngComm*, 2010, 12, 4365-4371.
6. Y. Xia, S. Li, B. Wu, Y. Liu and X.-J. Yang, *CrystEngComm*, 2011, 13, 5763-5772.
7. F. Ma, D.-B. Wei and Z.-M. Cao, *Acta Crystallogr. Sect E: Struct. Rep. Online*, 2012, 68, m611-m612.
8. C.-Q. Wan, S. A. Al-Thabaiti, X.-D. Chen and T. C. W. Mak, *Eur. J. Inorg. Chem.*, 2013, 30, 5265-5273.
9. C.-Q. Wan, Z.-W. Wang, G. Wang, A.-M. Li, Q.-H. Jin, Y.-H. Deng and T. C. W. Mak, *Eur. J. Inorg. Chem.*, 2013, 14, 2591-2600.
10. K. J. Wei, Y. S. Xie, J. Ni, M. Zhang and Q. L. Liu, *Inorg. Chem. Commun.*, 2006, 9, 926-930.
11. R. Benedix, *Z. Anorg. Allg. Chem.* , 1984, 24, 303.
12. M. A. Braverman, J. H. Nettleman, R. M. Supkowski and R. L. LaDuca, *Inorg. Chem.*, 2009, 48, 4918-4926.
13. G. A. Farnum, W. R. Knapp and R. L. LaDuca, *Polyhedron*, 2009, 28, 291-299.
14. E. L. Eliel, Wilen, Samuel H. Mander, Lewis N., *Stereochemistry of organic compounds* 1994, 1156.
15. D. B. Cordes, L. R. Hanton and M. D. Spicer, *Inorg. Chem.*, 2006, 45, 7651-7664.
16. A. D. Clark, *Z. Krist- New Cryst. St.*, 1998, 213, 382.

17. X. Z. Sun, H. J. Yan and C. Q. Wan, *Z. Krist- New Cryst. St.*, 2013, 228, 375-376.
18. B. Moulton and M. J. Zaworotko, *Chem. Rev.*, 2001, 101, 1629-1658.
19. D. A. McMorran, *Inorg. Chem.*, 2007, 47, 592-601.
20. L. Han and M. Hong, *Inorg. Chem. Commun.*, 2005, 8, 406-419.
21. R. Horikoshi, T. Mochida, N. Maki, S. Yamada and H. Moriyama, *Dalton Trans.*, 2002, 1, 28-33.
22. R. Carballo, B. Covelo, E. García-Martínez, A. B. Lago and E. M. Vázquez-López, *Polyhedron*, 2009, 28, 923-932.
23. D. H. Johnston and D. F. Shriver, *Inorg. Chem.*, 1993, 32, 1045-1047.
24. M. A. M. Abu-Youssef, V. Langer and L. Ohrstrom, *Dalton Trans.*, 2006, 21, 2542-2550.
25. I. R. Thomas, I. J. Bruno, J. C. Cole, C. F. Macrae, E. Pidcock and P. A. Wood, *J. Appl. Cryst.*, 2010, 43, 362-366.
26. I. J. Bruno, J. C. Cole, P. R. Edgington, M. Kessler, C. F. Macrae, P. McCabe, J. Pearson and R. Taylor, *Acta Crystallogr. Sect. B: Struct. Sci.*, 2002, 58, 389-397.
27. L. Yang, D. R. Powell and R. P. Houser, *Dalton Trans.*, 2007, 9, 955-964.
28. R. G. Serres, C. A. Grapperhaus, E. Bothe, E. Bill, T. Weyhermüller, F. Neese and K. Wieghardt, *J. Am. Chem. Soc.*, 2004, 126, 5138-5153.
29. E. C. Constable, C. E. Housecroft, M. Neuburger, S. Reymann and S. Schaffner, *Eur. J. Inorg. Chem.*, 2008, 22, 3540-3548.
30. E. C. Constable, C. E. Housecroft, B. M. Kariuki, M. Neuburger and C. B. Smith, *Aust. J. Chem.*, 2003, 56, 653-655.
31. P. L. Caradoc-Davies, L. R. Hanton and W. Henderson, *Dalton Trans.*, 2001, 19, 2749-2755.
32. M. Nishio, *Phys. Chem. Chem. Phys.*, 2011, 13, 13873-13900.
33. C. Janiak, *Dalton Trans.*, 2000, 21, 3885-3896.
34. C. A. Black, L. R. Hanton and M. D. Spicer, *Chem. Commun.*, 2007, 30, 3171-3173.
35. C.-Q. Wan, X.-D. Chen and T. C. W. Mak, *CrystEngComm*, 2008, 10, 475-478.
36. T. Bark and R. P. Thummel, *Inorg. Chem.*, 2005, 44, 8733-8739.
37. G. Yang, S. L. Zheng, X. M. Chen, H. K. Lee, Z. Y. Zhou and T. C. W. Mak, *Inorg. Chim. Acta*, 2000, 303, 86-93.
38. X. Hou, M. Schober and Q. Chu, *Cryst. Growth Des.*, 2012, 12, 5159-5163.
39. R. Singh, X. Hou, O. Molly, M. Schober and Q. Chu, *CrystEngComm*, 2012, 14, 6132-6135.
40. A. Bellusci, M. Ghedini, L. Giorgini, F. Gozzo, E. I. Szerb, A. Crispini and D. Pucci, *Dalton Trans.*, 2009, 36, 7381-7389.
41. A. Bellusci, A. Crispini, D. Pucci, E. I. Szerb and M. Ghedini, *Cryst. Growth Des.*, 2008, 8, 3114-3122.
42. R. P. Feazell, C. E. Carson and K. K. Klausmeyer, *Inorg. Chem.*, 2005, 45, 935-944.
43. G. M. Sheldrick, *SHELX97. Programs for Crystal Structure Analysis. Release 97-2. Institüt für Anorganische Chemie der Universität, Tammanstrasse 4, D-3400 Göttingen, Germany*, 1997.
44. Siemens, *SHELXTL. Structure Determination Software. Siemens Analytical X-ray Instruments Inc., Madison, Wisconsin, USA.*, 1995.
45. A. Altomare, M. C. Burla, M. Camalli, G. L. Cascarano, C. Giacovazzo, A. Guagliardi, A. G. G. Moliterni, G. Polidori and R. Spagna, *J. Appl. Cryst.*, 1999, 32, 115-119.
46. A. L. Spek, *PLATON. A Multipurpose Crystallographic Tool. Utrecht University, Utrecht, The Netherlands.*, 1999.
47. L. Farrugia, *J. Appl. Cryst.*, 1999, 32, 837-838.
48. C. F. Macrae, P. R. Edgington, P. McCabe, E. Pidcock, G. P. Shields, R. Taylor, M. Towler and J. van de Streek, *J. Appl. Cryst.*, 2006, 39, 453-457.

Table 3 Crystal and Structure Refinement Data for Complexes **I–IX**

Structure	**1**	**2**	**3**	**4**	**5**	**6**	**7**	**8**	**9**
Formula	$C_{24}H_{18}O_9N_4S_2F_6Ag_2$	$C_{22}H_{18}Ag_2Cl_2N_4O_{11}$	$C_{28}H_{27}Ag_2Cl_2N_7O_{11}$	$C_{28}H_{25}Ag_2Cl_2N_7O_{10}$	$C_{30}H_{28}Ag_2F_{12}N_8O_2P_2$	$C_{46}H_{34}O_{11}N_8S_2F_6Ag_2$	$C_{22}H_{16}AgBF_4N_4O_2$	$C_{22}H_{16}AgF_6N_4O_2P$	$C_{26}H_{22}AgF_6N_6O_2P$
Formula weight	900.28	801.04	924.21	906.19	1038.26	1268.67	563.07	621.23	703.34
Crystal System	Monoclinic	Monoclinic	Monoclinic	Monoclinic	Monoclinic	Monoclinic	Monoclinic	Monoclinic	Triclinic
Space group	*C*2/*c*	*C*2/*c*	$P2_1/c$	$P2_1/c$	$P2_1/c$	*C*2/*c*	$P2_1/c$	$P2_1/n$	*P*–1
a/ Å	13.7574(9)	12.4586(5)	7.5345(3)	7.8231(5)	7.9890(5)	27.5782(15)	11.020(11)	11.0709(7)	10.950(7)
b/ Å	11.2371(8)	9.8846(4)	19.1191(10)	18.8411(11)	22.9536(15)	10.6328(5)	18.3216(17)	18.5174(12)	11.1081(7)
c/ Å	19.0368(12)	21.2874(9)	23.0434(11)	22.8612(13)	20.1547(15)	18.6286(9)	10.7558(10)	11.6388(8)	12.1273(9)
α/°	90	90	90	90	90	90	90	90	85.248(2)
β/°	95.529(2)	102.7935(18)	92.045(1)	90.874(3)	91.046(3)	117.5172(17)	93.782(4)	96.473(3)	86.205(3)
γ/°	90	90	90	90	90	90	90	90	83.680(3)
V/Å^3	2929.3(5)	2556.6(18)	3317.4(3)	3369.3(5)	3695.3(6)	4844.8(6)	2167.4(5)	2370.8(3)	1458.7(2)
Z	4	4	4	4	4	4	4	4	2
T/K	90(2)	90(2)	90(2)	90(2)	90(2)	90(2)	90(2)	90(2)	90(2)
μ/mm–1	1.577	1.811	1.412	1.387	1.249	0.987	0.994	0.993	0.819
Total reflections	22,092	39,118	39,984	38,976	58,540	26,131	26,132	21,026	17,617
Unique reflections (R_{int})	8857 (0.0312)	9878 (0.0325)	9643 (0.0411)	9961 (0.0394)	9915 (0)	9998 (0.0538)	9900 (0.0347)	9898 (0.0210)	9112 (0.0289)
R_1 indices [$I>2\sigma(I)$]	0.0199	0.0285	0.0495	0.0687	0.0694	0.0596	0.0221	0.0340	0.0446
ω*R*2 (all data)	0.0522	0.1269	0.1158	0.1792	0.2414	0.1368	0.0559	0.0846	0.1247
Goodness-of-fit	1.088	1.209	1.069	1.066	1.149	1.150	1.083	1.145	1.082

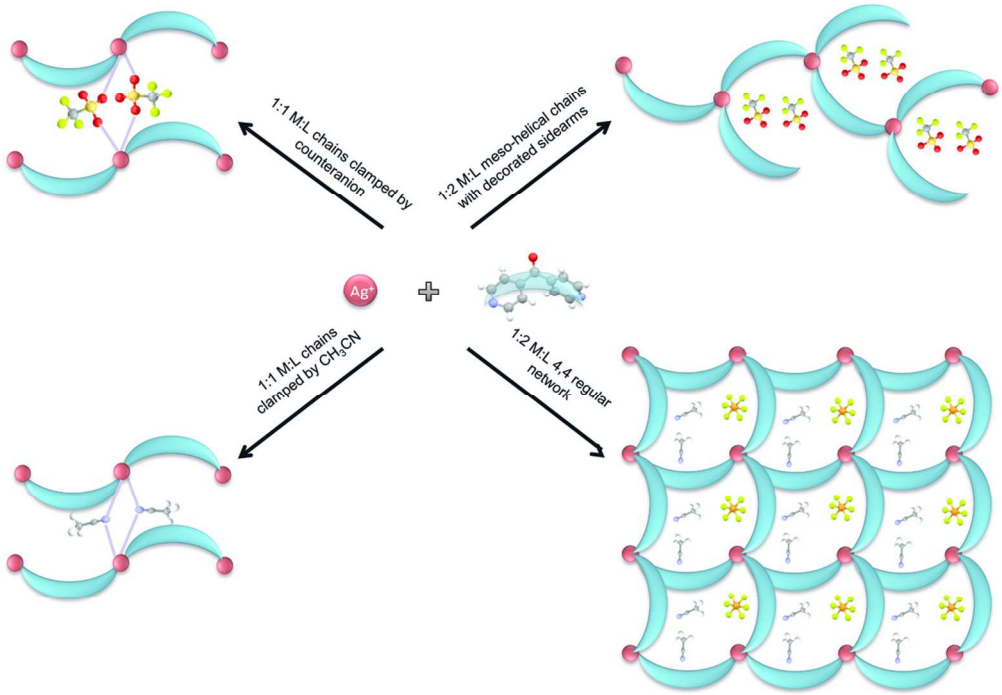

Two series of related coordination polymers of Ag(I) salts and L with varying M:L ratio (1:1 and 1:2) produce one series (1:1) of polymers that was not sensitive to counteranion and another (1:2) that displayed a remarkable sensitivity to counteranion showing a transition from ordered 1D meso-helical chains to 2D (4,4) nets.
102x72mm (300 x 300 DPI)